Chromosome Research (2007) 15:1061–1073
DOI: 10.1007/s10577-007-1181-7

Chromosome neighborhood composition determines translocation outcomes after exposure to high-dose radiation in primary cells

Lura Brianna Caddle[1], Jeremy L. Grant[2], Jin Szatkiewicz[1], Johann van Hase[3], Bobbi-Jo Shirley[1], Joerg Bewersdorf[4], Christoph Cremer[3,4], Alain Arneodo[4,5], Andre Khalil[2,4] & Kevin D. Mills[1,4]*
[1]*The Jackson Laboratory, 600 Maine street, Bar Harbor, ME 04609, USA; Tel: +1-207-288-6820; E-mail: Kevin.mills@jax.org;* [2]*Department of Mathematics & Statistics, University of Maine, Orono, ME 04469, USA;* [3]*Kirchhoff Institute for Physics, University of Heidelberg, D-69120, Germany;* [4]*Institute for Molecular Biophysics, University of Maine, Orono, ME 04469, USA;* [5]*Laboratoire Joliot Curie et Laboratoire de Physique, Ecole Normale Supérieure de Lyon (CNRS), 69364 Lyon Cedex 07, France*
** Correspondence*

Received 18 July 2007. Received in revised form and accepted for publication by Mary Delany 26 September 2007

Key words: chromosome positioning, nuclear domain, primary cells, p53, radiation, translocation

Abstract

Radiation exposure is an occupational hazard for military personnel, some health care professionals, airport security screeners, and medical patients, with some individuals at risk for acute, high-dose exposures. Therefore, the biological effects of radiation, especially the potential for chromosome damage, are major occupational and health concerns. However, the biophysical mechanisms of chromosome instability subsequent to radiation-induced DNA damage are poorly understood. It is clear that interphase chromosomes occupy discrete structural and functional subnuclear domains, termed chromosome territories (CT), which may be organized into 'neighborhoods' comprising groups of specific CTs. We directly evaluated the relationship between chromosome positioning, neighborhood composition, and translocation partner choice in primary lymphocytes, using a cell-based system in which we could induce multiple, concentrated DNA breaks via high-dose irradiation. We critically evaluated mis-rejoining profiles and tested whether breaks occurring nearby were more likely to fuse than breaks occurring at a distance. We show that CT neighborhoods comprise heterologous chromosomes, within which inter-CT distances directly relate to translocation partner choice. These findings demonstrate that interphase chromosome arrangement is a principal factor in genomic instability outcomes in primary lymphocytes, providing a structural context for understanding the biological effects of radiation exposure, and the molecular etiology of tumor-specific translocation patterns.

Abbreviations: Chr, chromosome; CT, chromosome territory; 2D, two-dimensional; 3D, three-dimensional; DSB, DNA double strand break; FND, fraction of the nuclear distance; HR, homologous recombination; IR, ionizing radiation; LOH, loss of heterozygosity; NHEJ, nonhomologous end joining

Introduction

Radiation is a major therapeutic agent in the treatment of a broad range of cancers and is critical for numerous medical imaging modalities. Thus patients, as well as personnel working in radiodiagnostic or radiotherapeutic areas, are likely to encounter radiation exposure. Radiation exposure is also an occupational risk for airport and other security screeners, military personnel, and individuals working in specific nuclear

applications. Understanding and minimizing the negative consequences of radiation exposure in patients and workers, while maximizing positive benefits requires a detailed understanding of radiobiological effects in cells.

While chromosomal instability is a major potential result of radiation exposure, the precise molecular and biophysical mechanisms by which radio-induced DNA damage is translated into chromosomal abnormalities, such as translocations, are not known. The two major pathways of DNA double strand break repair—homologous recombination (HR) and nonhomologous end joining (NHEJ)—must be appropriately coordinated and deployed both temporally and spatially. How this is accomplished in the context of three-dimensional (3D) nuclear organization is a matter of ongoing investigation. Errors in the proper regulation or coordination of these DSB repair mechanisms can lead to either failed or inappropriate repair, with the latter potentially creating translocations. In this context, 3D proximity of translocation donor and target sites must ultimately be required, at least transiently, for the fusion step to occur. It remains unknown, however, to what extent proximity contributes to translocation rate or target site selection. In interphase, chromosomes are not diffusely intermingled in the nucleus but occupy discrete structural and functional subnuclear domains, termed chromosome territories (CT), that are largely distinct but may overlap at their edges (Cremer & Cremer 2001, Parada & Misteli 2002, Parada *et al*. 2004a, b) CTs may be further organized into 'neighborhoods' comprising groups of CTs with characteristic radial and/or relative 3D positioning (Bickmore & Teague 2002, Arsuaga *et al*. 2004, Stadler *et al*. 2004, Berr *et al*. 2006, Meaburn & Misteli 2007, Meaburn *et al*. 2007).

Comparative mapping in several vertebrate species has revealed evidence for cell-or tissue-specific CT spatio-geometry, and suggested that 3D morphological changes may contribute to the dynamic repositioning of CTs during development or differentiation (Stadler *et al*. 2004). In the context of cancer, analyses of a mouse lymphoma model revealed proximate localization of translocation-prone chromosomes, and a number of studies have suggested that the frequency with which specific translocations are observed in certain cancers may correlate with the proximity of the participant chromosomes in corresponding normal cells (Bickmore & Teague 2002, Hlatky *et al*. 2002, Branco & Pombo 2006, Cornforth 2006, Meaburn *et al*. 2007). While these findings implicate chromosome proximity as a factor in translocation susceptibility, such studies have historically been subject to two limitations. First, translocation outcomes following irradiation have been assumed to reflect underlying CT positioning, but this assumption has remained largely untested. Second, characterization of CT positioning in specific cell types, which show unique translocation patterns following transformation, can be confounded by selection for or against certain translocations. Thus it can be difficult in such correlative studies to discern the true relationship between nuclear organization and oncogenic genome instability. In this context, the present study represents a key advance, because the use of cells deficient for the cell cycle/DNA damage checkpoint factor p53 (encoded by *Trp53*), permitted a high level of radioinduced chromosomal damage while minimizing the skewing effects of selection, allowing us to directly evaluate the extent to which native CT positions in undamaged interphase nuclei can dictate translocation outcomes. This important feature of the study permitted us to relate CT positioning *before* radiation exposure to translocation outcomes *after* irradiation. We now demonstrate that CT neighborhoods are made up of heterologous chromosomes, and that translocation outcomes are strongly linked to the distances between heterologous CTs. These findings support the hypothesis that interphase chromosome positioning plays a key role in the outcomes of genomic instability following radiation exposure.

Materials and methods

Mice

Primary pro-B cells were obtained from wild-type C57BL/6J or $Trp53^{-/-}$mice (Donehower *et al*. 1992). Mice were maintained on standard chow (Lab Diet) in pressurized, individually ventilated (PIV) caging. Bone marrow donors were euthanized by CO_2 inhalation at 6–12 weeks of age. $Trp53^{-/-}$ mice were generated by $Trp53^{+/-}$ intercrosses. Genomic DNA for genotyping was obtained from weanling tail tips. $Trp53^{-/-}$genotyping was performed by PCR in

25 μl reaction volumes, with the following cycle parameters: 94°C for 4 min. followed by 35 cycles of 94°C, 20 s; 55°C, 20 s; 72°C, 40 s; and a final incubation at 72°C for 10 min. Wild-type and mutant bands (320 bp and 150 bp, respectively) were amplified in separate reactions with the following primers:

WT fwd (GTGTTTCATTAGTTCCCCACCTT GAC);
WT rev (ATGGGAGGCTGCCAGTCCTAACCC);
Mutant fwd (GTGGGAGGGACAAAAGTTCGA GGCC);
Mutant rev (TTTACGGAGCCCTGGCGCTCGA TGT)

Cell culture

Either normal or *Trp53*$^{-/-}$ primary pro-B cells were obtained from appropriate femur-derived total bone marrow. Both femurs of donor mice were flushed with growth medium (RPMI 1640 medium containing 15% fetal bovine serum, 20 mM Hepes, 2 mM L-glutamate, penicillin/streptomycin) supplemented with 25 ng/ml IL-7 (R&D systems, Minneapolis, MN, USA). Cells were resuspended at a concentration of 1–2×10^6 cells/ml in growth medium with IL-7, and cultured for 6–8 days. Enrichment for the pro-B cell fraction was verified by flow cytometric analysis, staining for cell surface expression of the B-lineage markers B220/CD45R, IgM, CD19, and CD43. All flow cytometry was performed using a Becton-Dickinson FACSCalibur cytometer outfitted with CellQuest Pro software. Typical cultures yielded 60–80% pro-B cells by day 7. Further purification was accomplished by automated magnetic bead-based cell sorting (AutoMACS; Miltenyi Biotec), for B220$^+$ IgM-cells, according to the manufacturer's sorting protocol. As an alternative method, pro-B cells were sorted directly from total bone marrow of 6–12-week-old mice, by first depleting for IgM-expressing cells, then sorting for B220$^+$ cells.

FISH

For chromosome painting, pro-B cells were adhered to poly(L-lysine)-coated slides, permeabilized briefly in ice-cold CSK (100 mM NaCl, 300 mM sucrose, 10 mM Pipes pH7.4, MgCl 3 mM, 0.025% Triton X-100), and fixed in 4% formaldehyde/1×phosphate-buffered saline. Slides were rinsed in room-temperature 70% ethanol, and used immediately or stored in 70% ethanol at 4°C. Compatible pairs of fluorescently labeled (rhodamine or FITC) mouse chromosome specific paints (Applied Spectral Imaging, Vista, CA, USA) were concomitantly hybridized to fixed cells as follows: 8 μl each of a rhodamine- and FITC-labeled paint were premixed, applied to a dried slide containing fixed cells, coverslipped, and placed on an 80°C heat block for 2 min; coverslips were sealed with rubber cement, and slides were incubated in a humidified chamber at 37°C for 24–36 h, in the dark. Slides were washed three times with 0.2×SSC/0.1% Tween-20 for 20 min per wash at 74°C, followed by a final 10 min wash in 4×SSC/0.05% Tween-20 at room temperature. Slides were mounted with Vectashield containing DAPI counterstain (Vector Laboratories, Burlingame, CA, USA), sealed with nail polish, and imaged or stored upright at −20°C. Widefield imaging was carried out on an automated Nikon 90i upright microscope outfitted for epifluorescence using 60×or 100×1.4 NA oil immersion PlanApo objectives, and IPLab image acquisition software (BD Biosciences, Rockville, MD, USA). Multiple focal planes traversing the depth of the nucleus, as judged by DAPI staining, were acquired and digitally combined by two-dimensional maximum fluorescence intensity projection using IPLab scripts. Confocal microscopy was performed using a Leica SP2 laser scanning confocal microscope equipped with a 100×, 1.4 NA oil PlanApo objective and with the pinhole set to 1 Airy disk. Image stacks containing full nuclear volume data were acquired by traversing from top to bottom in 0.2 μm steps, yielding stacks of 40–70 optical sections.

Image analysis

For all images, except for object segmentation, minimal postacquisition image processing was performed. Where necessary, nuclear boundaries, as determined by either DAPI staining or background fluorescence, are indicated by a digitally overlaid line. For automated and semi-automated image analysis, two-dimensional (2D) maximum fluorescence intensity projections were generated for each image using IPLab software (BD Biosciences). These were subsequently segmented using the Wavelet Transform Modulus Maxima (WTMM) algorithm, a

multi-fractal tool for intensity-independent object identification that locates edge detection lines based on image gradient (Khalil *et al*. 2007).

Irradiation and spectral karyotyping

For spectral karyotyping (SKY) analysis, *Trp53*$^{-/-}$ pro-B cells were exposed to 12.5 Gy of γ-irradiation using a Cs^{137} source and allowed to recover for 24 h. Cells were incubated in the presence of 40 ng/ml colcemid (Karyomax; Invitrogen) for approximately 6 h, to enforce metaphase arrest. Cells were transferred to a warmed hypotonic potassium chloride solution (75 mM) for 7 min, and fixed by two changes of cold 3:1 methanol–acetic acid. Metaphase chromosomes were applied to slides and dried for 3–7 days prior to hybridization with mouse chromosome SKY paints (Applied Spectral Imaging), according to the manufacturer's protocol. Spectral karyotypes were obtained on a complete ASI Cytogenetics Workstation equipped with automated stage, SpectraCube imaging head, and dedicated software for imaging and archiving.

Statistical methods

Normal and *Trp53*$^{-/-}$ datasets were tested for differences in chromosome positioning patterns by chi-squared heterogeneity testing and by application of log-linear modeling. Several approaches were used to analyze chromosome translocation frequencies. Chromosome lengths and gene content were determined based on NCBI Build 36 of the mouse genome, and gene density was subsequently defined as: Number of genes/length in megabase pairs (Mbp). The influence of chromosome length on the distribution of translocations was evaluated by correlation analysis, and by simple linear or log-linear regression testing. To determine whether the pairwise translocation data (see Figure 4) showed a random distribution, the observed translocation rates were compared with the predicted uniform rate using a random model in which each event was equally probable. Overall and subdivided chi-squared analyses were used for model fitting to detect discrepancy between observed and predicted values. Robust *p*-values were computed using Monte Carlo simulations in 100 000 replicates, and adjusted for multiple testing (Hope 1968, Hochberg 1988).

Results

Chromosome territory neighborhoods comprise heterologous clusters

As the first step toward assessing the role of nuclear architecture in chromosome instability it was necessary to determine relative CT positioning relationships in undamaged primary cells. For this purpose, we focused on primary B-lymphoid cells, and investigated the positioning of the following pairwise combinations of chromosomes (Chrs), chosen on the basis of chromosome size, gene density, or their known involvement in cancer-associated translocations, using a chromosome painting approach: Chrs 1+12; 1+15; 6+15; 12+15; 11+19; and 15+19. Two-dimensional, channel-merged maximum fluorescence intensity (MFI) projections were scored, to assign chromosome territory distribution into one of four categories: (I) all chromosomes dispersed; (II) proximal positioning of at least one pair of homologues; (III) proximal positioning of at least one pair of heterologues; and (IV) clustering of all four chromosomes (Figure 1A,B). We found that, overall, heterologous groupings (category III) represented the most frequent CT arrangement, observed in approximately 60–80% of cells. Notably, heterologous CT groupings occurred, on average, over 4-fold more often than homologous groupings (Category II), 8-fold more often than four-way clustering (IV), and 11-fold more often than four-way dispersal (I) (Figure 1C). These results indicate that nuclear organization, in primary lymphocytes, favors arrangements of nearby heterologous chromosomes, and generally disfavors proximal localization of homologous chromosomes.

Inter-heterologue distance correlates with frequency of edge overlap

From these findings, we reasoned that any given chromosome should be distributed, on average, measurably closer to heterologous CTs than to their homologous counterparts. Thus, to quantify the heterologous CT grouping phenomenon, edge-to-edge distances for heterologous chromosomes, as well as the corresponding homologous pairs, were measured. To obtain edge-to-edge measurements, we employed wavelet-based segmentation to locate

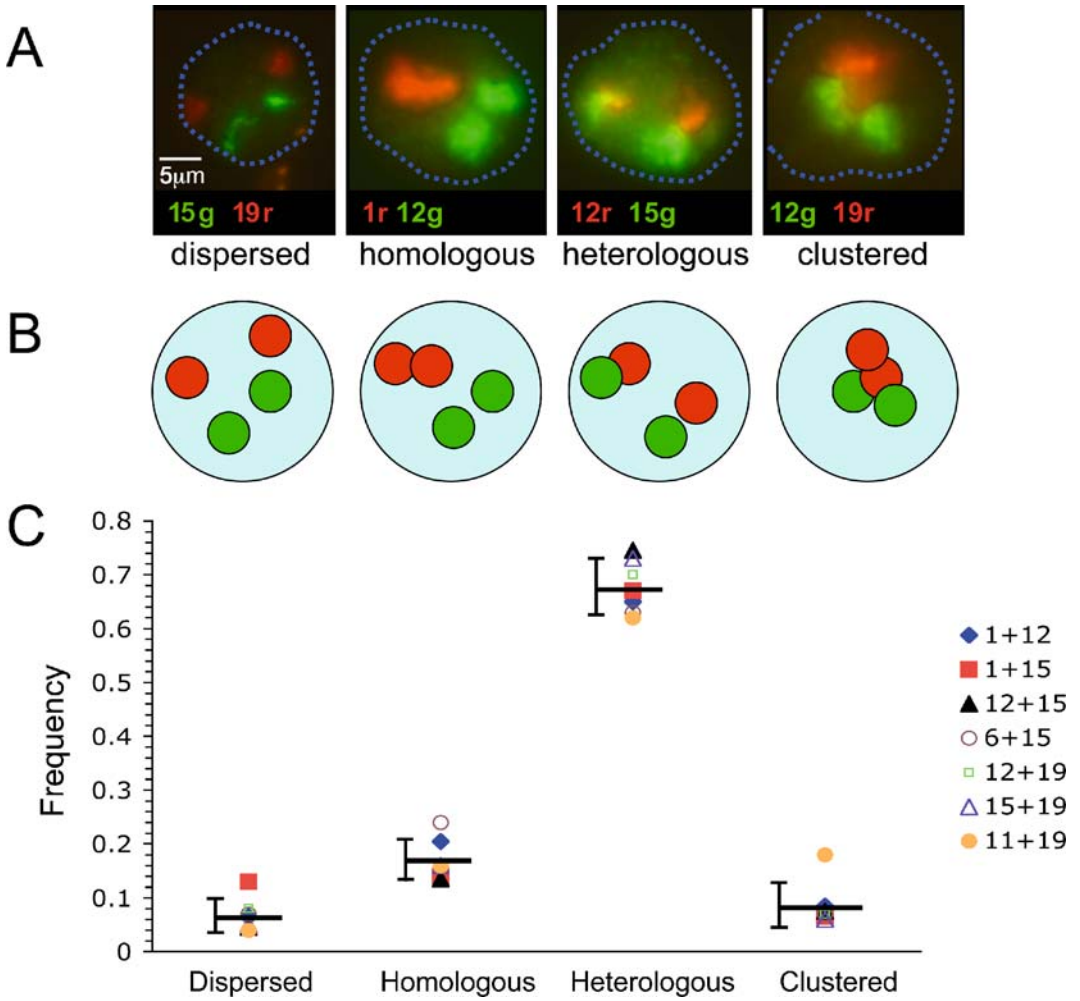

Figure 1. Chromosome territories form heterologous clusters in pro-B cell interphase nuclei. (A) Sample images of pro-B cell nuclei stained for specific chromosome pairs, indicated below each image. Shown are examples of the observed CT grouping patterns: dispersed, homologous, heterologous, and clustered. Individual CTs were painted with the designated colors and the nuclear boundary is indicated by the blue overlaid line. (B) Diagrammatic representation of CT positioning categories. (C) The frequency of each chromosome positioning category, as a function of the total number of cells analyzed for each chromosome pair, was determined for the indicated chromosome pairs. The horizontal bar in each category represents the average value for all chromosomes (error bar=standard deviation).

object boundaries by scanning for edge detection lines (Figure 2A) (Khalil *et al*. 2007). The nearest inter-CT distances were calculated from the same interphase CT images used for the analyses above. Measurements were expressed as a fraction of the nuclear diameter (FND) (Figure 2B). As predicted from the observations above, heterologous chromosome pairs exhibited shorter average inter-CT distances (FND<0.25) than the corresponding pairs of homologous chromosomes (FND $\approx$ 0.27), although both categories showed broad and overlapping ranges for individual measurements (Figure 2B). As an additional measure of heterologue proximity, we also assessed the frequency of inter-CT edge overlaps, reasoning that shorter average inter-CT distances should also correspond with higher overlap frequencies. The frequency of edge overlaps correlated directly with the inter-CT distances measured above. Chromosomes 11 and 19 showed both the shortest average inter-CT distance (FND $\approx$ 0.224), and the highest overlap frequency (0.889). By contrast, chromosomes 1 and 12 showed the greatest average inter-CT distance

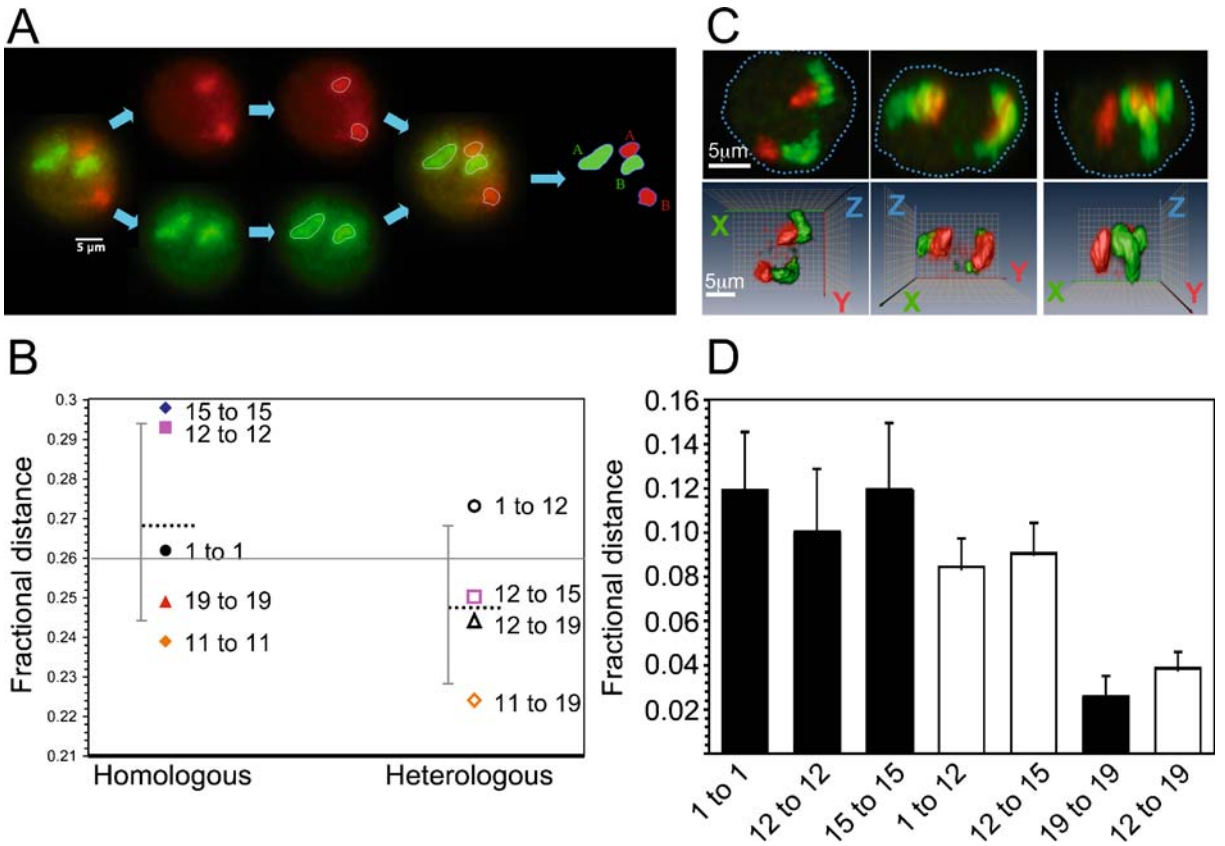

Figure 2. Heterologous chromosomes are positioned closer and overlap more frequently than homologous chromosomes. (A) Two-dimensional maximum fluorescence intensity (MFI) projection of chromosomes 12 (red) and 15 (green), imaged by widefield, epifluorescence microscopy. Different color channels were acquired separately, segmented using the Wavelet Transform Modulus Maxima approach, and digitally combined (IPLab software) to produce color-merged images with demarcated CT boundaries. These were used to identify individual objects for subsequent distance or overlap measurements. (B) Inter-CT distance for homologous (filled symbols) or heterologous (open symbols) CTs was calculated. Average distances for specific CT pairs are plotted as a fraction of the nuclear diameter (FND), to account for variations in overall nucleus size. Average of all homologous or heterologous measurements, respectively, is indicated by a dashed line (error bar=standard deviation). The mean of all measurements (FND ≈ 0.26) is indicated by a solid line, spanning the plot. (C) Laser scanning confocal micrographs of Chrs 1 (green) and 12 (red). Upper panels show 2D projections in the *XY*, *YZ*, and *XZ* planes (left to right). Lower panels show corresponding 3D surface-rendered reconstructions (Amira). Grid=1 μm. (D) Inter-CT distances, for each of the chromosome pairs measured, expressed as a fraction of the nuclear diameter, and classified as either homologous (filled bars) or heterologous (open bars) pairs. (Error bars=95% CI.)

Figure 3. IR-induced chromosome damage and translocation is dependent on chromosome length. (A) Survival of primary wild-type versus primary *Trp53*$^{-/-}$ cells after radiation exposure. Cells were exposed to either 0 (green bars) or 12.5 Gy (red bars) ionizing radiation, allowed to recover in culture for 19 h, and then scored for surviving (Trypan blue-excluding) cells. Survival is expressed as the fraction excluding Trypan blue relative to the total cell count. (B) Primary *Trp53*$^{-/-}$ pro-B cells were exposed to 12.5 Gy of ionizing radiation, as in (A), and allowed to recover for 24 h in culture. Chromosome structural abnormalities, including fragments and translocations, were identified by spectral karyotyping (SKY), and quantified. Numerical aberrations without an associated translocation were not counted. Shown are the spectral, DAPI, and computer-classified images of a typical metaphase spread (upper panels) and the karyotype table (lower panel). (C) Number of translocations (black circles) and number of chromosome fragments (red circles) for each chromosome were measured by SKY, following irradiation. Circle size represents 95% confidence interval for each data set. Black and red lines indicate linear fit for corresponding data sets. *N*=80 nuclei. (D) Number of translocations and fragments were measured as a function of chromosome length (Mb). Selected chromosomes are indicated. Symbols are as in (C). (E) Number of translocations and fragments were measured as a function of gene density (number of genes/Mb). Selected chromosomes are indicated. Symbols are as in (C).

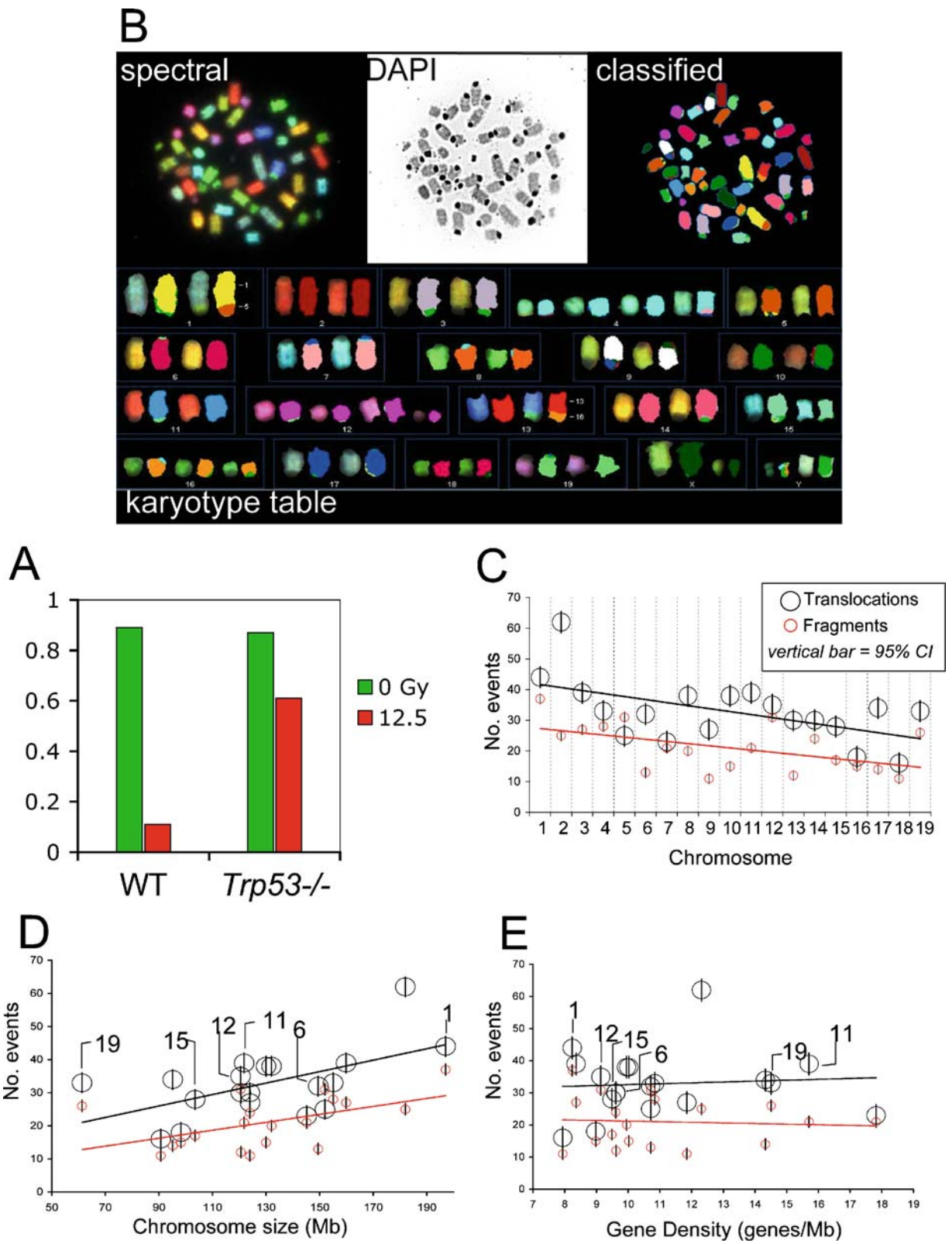
B
spectral
DAPI
classified
karyotype table
A
1
0.8
0.6
0.4
0.2
0
0 Gy
12.5
WT
Trp53-/-
C
Translocations
Fragments
vertical bar = 95% CI
No. events
Chromosome
D
No. events
Chromosome size (Mb)
E
No. events
Gene Density (genes/Mb)

(FND>0.27) and the lowest frequency of overlap (0.567). Together, these data confirm that heterologous chromosomes are distributed, on average, closer to one another than are the corresponding homologous chromosomes, and show that some specific heterologous pairs exhibit closer inter-CT distances and more frequent edge overlaps than others.

Heterologous chromosome clusters occur in three dimensions

While computational modeling indicates that accurate 3D positioning information can be extracted from 2D projected images (Khalil *et al*. 2007), such as those generated here, we wished to directly evaluate CT positioning in true 3D data. Serial optical sections were obtained via laser scanning confocal microscopy to acquire full nuclear volume data for the chromosome pairs 12+15 and 1+12 (control), and 12+19 (control). Resulting image stacks were used to derive three-dimensional (3D) nuclear reconstructions for inter-CT distance measurements. An example of a nucleus stained for chromosomes 1 and 12 is shown in Figure 2C. Between 25 and 40 such reconstructions were produced for each chromosome territory pair, and these were used to carry out all inter-CT measurements. As in the analyses above, inter-CT distances were expressed as a fraction of the nuclear diameter, to normalize for variations in nuclear size. Consistent with the findings described above, the 3D edge-to-edge measurements, while broadly overlapping, revealed a general preference for heterologue over homologue proximity (Figure 2D).

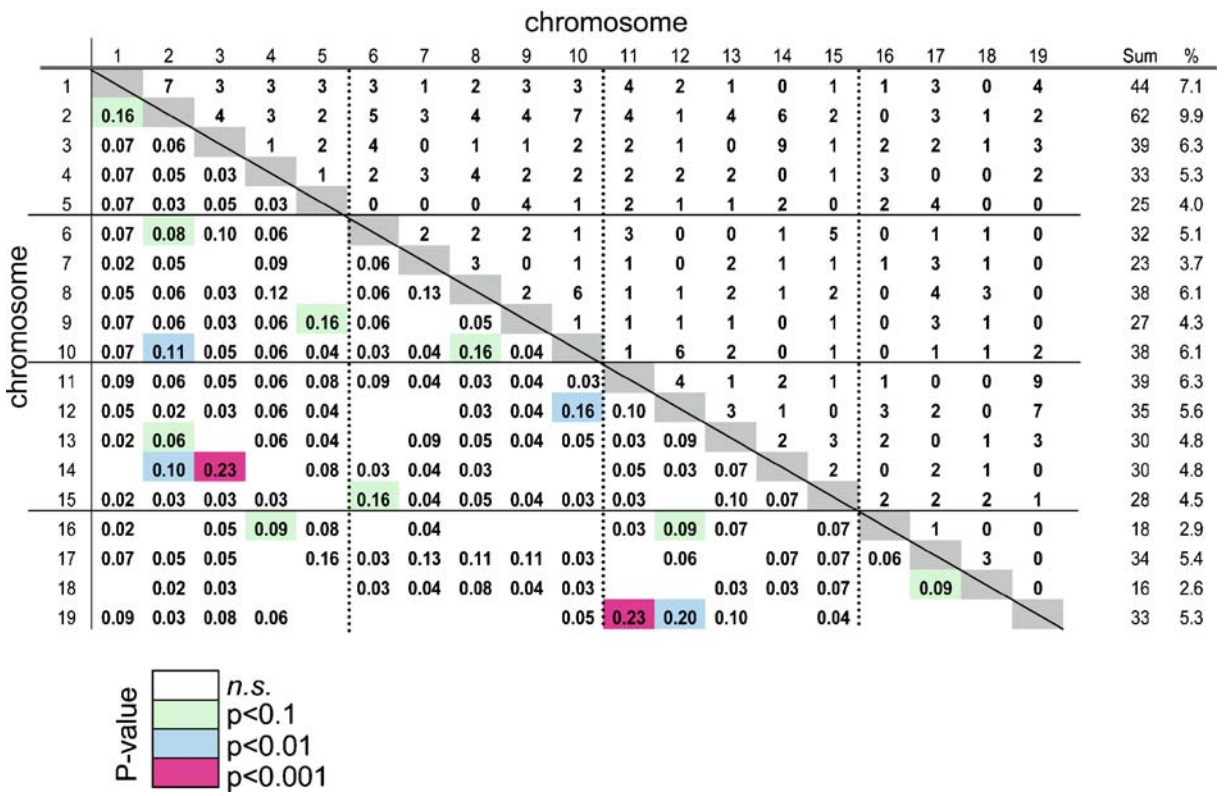

Figure 4. Spectral karyotype analysis of ionizing radiation-induced pairwise translocations. All possible pairwise translocations were tallied in a total of 80 pro-B cell nuclei, derived from 5 independent mice. The total number of times each translocation was observed is indicated above the diagonal line. Single chromosome translocation totals are indicated at the right (Sum) for each chromosome. The frequencies for each specific translocation, as a fraction of the single chromosome translocation total for the chromosome indicated at the left, are shown below the diagonal line. Statistical testing was performed by comparison of the observed rate with the predicted uniform rate using a random model. *p*-Values were adjusted for multiple testing and are indicated by color-coding, as shown below the matrix (Hochberg 1988).

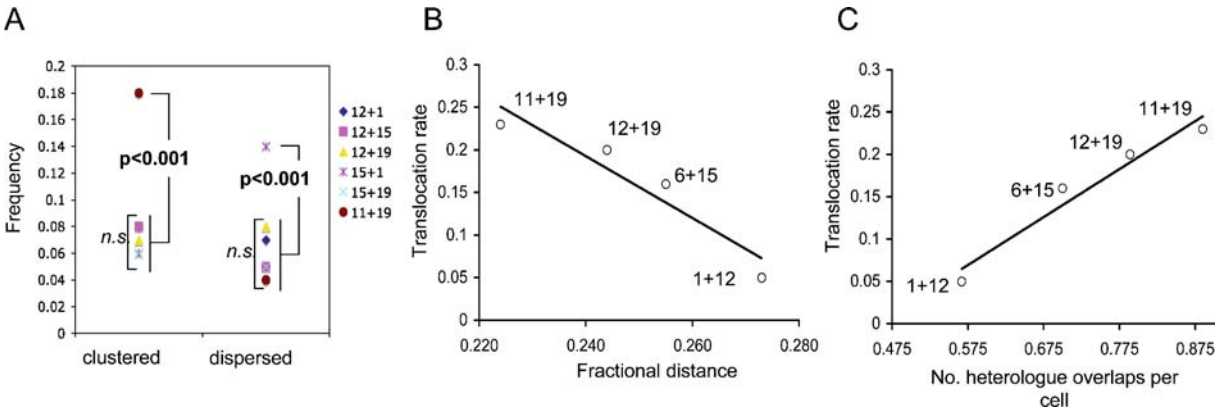

Figure 5. IR-induced translocation rate is directly dependent on inter-heterologue distance. (A) The frequency of CT clustering versus CT dispersion, as defined in Figure 1, is shown for the indicated heterologous chromosome pairs. Multiple pairwise testing reveals significant differences in the clustering of 11+19 (p=0.001) or dispersion of 1+15 (p=0.001) as compared with other tested chromosome pairs. Translocation rates, as shown in Figure 4, are indicated for Chrs 11+19 and Chrs 1+15. n.s., not significant (p>0.1). (B) Specific translocation rate for the indicated chromosome pairs, as determined in Figure 4, is plotted as a function of the fractional distance (fraction of nuclear diameter, FND). Line indicates linear fit. (C) Translocation rate (Figure 4) for the same chromosome pairs as in (B) is plotted as a function of heterologue overlaps. Line indicates linear fit.

Translocation rates are proportional to chromosome size and strongly correlate with chromosome positioning

Induction of chromosomal translocations is one possible biological consequence of radiation exposure, and is a clinical concern for the use of radiation as a diagnostic or therapeutic tool. Thus it is critical to understand how nuclear architecture may influence the biological effects of radiation. To test whether the likelihood of specific translocations, following exposure to high doses of ionizing radiation (IR) , is related to the initial positioning of the two partners, we performed a spectral karyotype analysis of irradiated primary lymphocytes. Our initial attempt, focusing on wild-type cells exposed to a range of IR doses (1, 5, or 12.5 Gy), failed to produce a high yield of metaphase spreads, probably owing to p53-dependent checkpoint responses to genotoxic damage (data not shown). Consistent with this notion, we found that *Trp53*-null cells showed a much higher rate of survival than normal cells following exposure to the highest IR dose (12.5 Gy) (Figure 3A). We therefore employed primary lymphocytes from p53-null mice to assess translocation outcomes. This key aspect of our experimental design permitted the efficient recovery of IR-induced translocations without the confounding effects of selection, allowing an unbiased evaluation of the CT positioning–translocation relationship. Pro-B cell preparations were obtained from 5 independent mice, exposed to 12.5 Gy of gamma (γ)-irradiation, and processed for spectral karyotyping after 24 h of recovery in culture. In a total of 80 nuclei, 399 individual autosome fragments and 312 autosome translocations (involving 624 translocation partners) were observed, yielding measured rates of approximately 5 fragments and 4 translocations per nucleus. Both the translocation and fragmentation frequencies scaled with the linear size of the individual chromosomes, but were not directly dependent on gene density (Figure 3C–E).

To evaluate translocation partner choice for specific translocations, all possible pairwise translocation rates were determined (Figure 4). This revealed that, while most translocations occurred essentially at random, several specific translocations occurred at significantly higher frequencies (Figure 4). Strikingly, the frequency of these translocations correlated with the positioning and average proximity of the participating CTs in un-irradiated nuclei (Figure 5). Chromosomes 11+19 exhibited a significantly higher rate of proximal grouping than any other chromosome pair tested (p<0.001), and also showed the highest overall translocation rate (0.23) (Figures 4 and 5A). Conversely, chromosomes 1+15, which displayed a significantly higher frequency of complete dispersal relative to any other chromosome pair tested (p<0.001), exhibited a measurably low trans-

location rate (0.02) (Figures 4 and 5A). In support of this finding, specific translocation rates also scaled with both the inter-CT distance and edge-overlap frequencies, where closer average distance translated into higher translocation frequency (Figures 4 and 5B, C). Consistent with the observation that single chromosome translocation rates were independent of the overall gene density, the frequencies of specific pairwise translocations were also independent of the aggregate gene density for the participating chromosome pair (data not shown). Thus, the likelihood of DNA damage-induced translocation between specific chromosomes is related to the relative proximity of those chromosomes prior to damage, irrespective of the overall whole-chromosome concentration of genes on either translocation partner.

Discussion

Here we have shown that, in primary B-lineage lymphocytes, positioning of chromosome territories in interphase nuclei favors the creation of CT neighborhoods comprising heterologous chromosomes. One key feature of this organization is that proximal clustering of homologous chromosomes is strongly disfavored. We further show that positioning into heterologous CT neighborhoods is likely nonrandom, suggesting that CTs are actively sorted into heterologous neighborhoods. Finally, we present direct evidence that the composition of such heterologous CT neighborhoods influences translocation proclivity, following exposure to high-dose ionizing irradiation. The latter finding is significant because it confirms the 'proximity first' hypothesis for translocation mechanism, which posits that chromosome positioning is sufficient to determine the likelihood of interaction between any two chromosomes.

Heterologous chromosome territory neighborhoods

It has become increasingly appreciated that mammalian interphase chromosomes are not diffusely intermingled within the nucleus, but rather occupy discrete structural and functional domains (Cremer *et al*. 2000, Cremer & Cremer 2001, Dundr & Misteli 2001, Gilbert *et al*. 2005). Whether whole chromosome territories are further organized into specific arrangements, however, and by what mechanisms, remain open and controversial questions. In this context we now show that CT positioning favors groupings of heterologous chromosomes and disfavors groupings of homologous chromosomes. Mechanistically, heterologous CT neighborhoods may be expected by random positioning, because the number of possible heterologous pairings of two chromosomes vastly outnumbers the possible homologous pairings (760 versus 20, respectively). However, comparisons of our empirical positioning data with a series of observation-based random-positioning computational models reveal nonrandom CT localization (Khalil *et al*. 2007). Moreover, a number of studies have suggested that CTs are actively positioned by partitioning of gene-rich chromosomes to the nuclear center and gene-poor chromosomes to the nuclear periphery, leading to characteristic groupings of chromosomes according to gene density (Bickmore & Teague 2002, Cornforth *et al*. 2002, Tanabe *et al*. 2002, Cremer *et al*. 2003, Gilbert *et al*. 2004, Kreth *et al*. 2004, Thomson *et al*. 2004, Murmann *et al*. 2005, Mora *et al*. 2006, Meaburn & Misteli 2007). Such partitioning would thus lead to natural groupings of chromosomes according to gene density. In spite of this trend toward density-dependent chromosome positioning, our data suggest that the rate of individual radiation-induced translocations in p53-deficient cells is, at best, indirectly related to the overall gene density on either of the participating chromosomes. This finding may indicate that other mechanisms, in addition to gene density, also critically influence chromosome positioning as well as translocation susceptibility. Alternatively, it is possible that local concentrations of genes, even on overall gene-poor chromosomes, could produce specific hotspots for translocations that would appear to be independent of overall gene density. In such cases, co-localization of specific chromosome regions, perhaps as a consequence of transcriptional activity, could predispose certain locations to instability. It will be interesting to further test this notion in the context of IR-induced damage by assessing whether such induced translocations show preferential breakpoints on specific chromosomes and whether these correlate with particular genome organizational features. In this context, karyotype analyses based on chromosome G-banding would provide a first-level indication of preferen-

tially breakpoint clustering, but would be insufficient to determine co-association with specific genome features. To accomplish the latter will require a combination of both cytogenetic and molecular analyses, including high-throughput cloning and sequencing of a large number of translocation junctions.

In terms of CT positioning, gene density may play a general role in the patterns of nuclear organization observed here, but additional factors are also required because heterologous groupings predominated over homologous groupings, even in cases where the homologous pair contained overall higher gene density than the heterologous pair. One likely factor is co-association of genes on different chromosomes in common nuclear locations. One recently published study that may support this notion showed that the *Myc* gene, a frequent target for translocation with the immunoglobulin heavy chain locus (*Igh*) in many B-lineage neoplasms, is preferentially relocated into proximity with a transcriptional active *Igh* locus , via co-association with the same transcription factory (Osborne *et al*. 2007). Such associations may be critical for coordinated expression or proper regulation of functionally related genes. Because there are four times as many possible configurations for pairs of genes on heterologues as there are for pairs on homologues, such co-association may favor proximal arrangements of heterologous CTs. Thus, genome organization may partially influence higher-order nuclear architecture. Indeed, it has recently been shown that the linear organization of genomic features along a portion of mouse chromosome 14 can be correlated with the 3D folding properties of that segment in the interphase nucleus (Shopland *et al*. 2006). We have also observed, for all chromosomes examined, an average ellipsoidal morphology (Khalil *et al*. 2007). In this regard, another intriguing possible mechanism for establishing nuclear architecture may derive from sphere packing theory. For random packing arrangements, it has been shown that ellipsoids can pack more densely, and share more points of contact with other objects, than can uniform spheres (Donev *et al*. 2004, Chaikin *et al*. 2006). Thus, the ellipsoidal morphology of interphase CTs could perhaps facilitate maximal space occupancy while permitting the greatest number of interchromosomal contacts, and thus contribute to CT neighborhood organization.

Implications of heterologous groupings

In addition to locating gene-dense chromosomes into transcriptionally active nuclear sub-compartments, what might be the effect of positioning interphase CTs into heterologous neighborhoods? Given that chromosome proximity is required for translocations to occur, close proximal groupings of heterologous CTs would seem to increase the risk, following DNA damage, of inappropriate recombination occurring between nonhomologous chromosomes. NHEJ, one of the two main DSB repair mechanisms in mammalian cells, normally catalyzes the rejoining of cognate broken DNA ends, irrespective of sequence homology flanking the break. However, this pathway can also effect the mis-repair of noncognate ends, which can result in large-scale genome rearrangements, such as vast deletions or chromosomal translocations. In this context, heterologous CT neighborhoods, such as those described here, may provide a nidus for the formation of translocations via NHEJ, especially in instances of significant heterologue intermingling. This may be particularly relevant during the G_1 phase of the cell cycle, where NHEJ is thought to predominate over homologous recombination (HR) in the repair of DSBs, or in cases where a high level of damage throughout the nucleus would prevent relocalization of sparse breaks to centers of repair (Aten *et al*. 2004). Conversely, heterologous neighborhoods may result in some level of protection against loss of heterozygosity (LOH) via recombination between homologues. In this regard, neighborhoods of heterologous chromosomes may be thought of as a buffer zone against inappropriate interactions between homologous chromosomes, where HR-mediated repair could result in LOH via gene conversion, leading to allele replacement. This mechanism might be especially important during postreplicative (late S or G_2) stages of the cell cycle, when both NHEJ and HR are active, and thus there is a larger danger of inappropriate homologue–homologue interactions (Couedel *et al*. 2004, Mills *et al*. 2004). Because LOH is thought to be a key tumor-initiating event in many cancers, such buffering of homologue interactions in interphase nuclei may help to prevent or forestall this form of chromosomal instability. Because the irradiated cells in this study were asynchronously growing at the time of irradiation, it is likely that both G_1 and G_2 influences were

at play, and thus translocations could have occurred pre and/or post replication. In this context, NHEJ would be readily capable of generating interchromosomal rearrangement, but it is not clear whether HR would similarly catalyze recombination between patches of local homology on nonhomologous chromosomes. However, either mechanism could produce the observed translocations. In this regard, a major, current question in the field of DSB repair is how the two major pathways—HR and NHEJ—are spatially and temporally regulated and coordinated. Perhaps the 3D organization of CTs in the nucleus provides a measure of such regulation, by disfavoring potentially deleterious interaction between homologues and/or promoting nonhomologous repair when and where appropriate.

A more speculative possibility regarding the consequences of heterologous CT organization is that, over evolutionary timescales, heterologous groupings might influence which chromosomes exchange with others as chromosomal units become rearranged during genome evolution. It will be interesting to combine comparative genomics with species-specific CT positioning studies to determine whether some CT positioning relationships may be evolutionarily conserved, and whether CT positioning relationships reflect how chromosomes have become rearranged during mammalian evolution.

Acknowledgements

We are grateful to Will Schott and Mark Lessard for technical advice and assistance. We also thank Sarah Maas, Lindsay Shopland and Mary Ann Handel for discussions and critical comments. The authors do not have commercial interests or a conflict of interest pertaining to the work described herein. This work was supported, in part, by a Jackson Laboratory Cancer Center Pilot Study Grant (K.D.M).

References

Arsuaga J, Greulich-Bode KM, Vazquez M ***et al.*** (2004) Chromosome spatial clustering inferred from radiogenic aberrations. *Int J Radiat Biol* **80**: 507–515.

Aten JA, Stap J, Krawczyk PM *et al.* (2004) Dynamics of DNA double-strand breaks revealed by clustering of damaged chromosome domains. *Science* **303**: 92–95.

Berr A, Pecinka A, Meister A *et al.* (2006) Chromosome arrangement and nuclear architecture but not centromeric sequences are conserved between *Arabidopsis thaliana* and *Arabidopsis lyrata*. *Plant J* **48**: 771–783.

Bickmore WA, Teague P (2002) Influences of chromosome size, gene density and nuclear position on the frequency of constitutional translocations in the human population. *Chromosome Res* **10**: 707–715.

Branco MR, Pombo A (2006) Intermingling of chromosome territories in interphase suggests role in translocations and transcription-dependent associations. *PLoS Biol* **4**: e138.

Chaikin PM, Donev A, Man W, Stillinger FH, Torquato S (2006) Some observations on the random packing of hard ellipsoids. *Ind Eng Chem Res* **45**: 6960–6965.

Cornforth MN (2006) Perspectives on the formation of radiation-induced exchange aberrations. *DNA Repair (Amst)* **5**: 1182–1191.

Cornforth MN, Greulich-Bode KM, Loucas BD *et al.* (2002) Chromosomes are predominantly located randomly with respect to each other in interphase human cells. *J Cell Biol* **159**: 237–244.

Couedel C, Mills KD, MBarchi KD *et al.* (2004) Collaboration of homologous recombination and nonhomologous end-joining factors for the survival and integrity of mice and cells. *Genes Dev* **18**: 1293–1304.

Cremer T, Cremer C (2001) Chromosome territories, nuclear architecture and gene regulation in mammalian cells. *Nat Rev Genet* **2**: 292–301.

Cremer T, Kreth G, Koester H *et al.* (2000) Chromosome territories, interchromatin domain compartment, and nuclear matrix: an integrated view of the functional nuclear architecture. *Crit Rev Eukaryot Gene Expr* **10**: 179–212.

Cremer M, Kupper K, Wagler B *et al.* (2003) Inheritance of gene density-related higher order chromatin arrangements in normal and tumor cell nuclei. *J Cell Biol* **162**: 809–820.

Donehower LA, Harvey M, Slagle BL *et al.* (1992) Mice deficient for p53 are developmentally normal but susceptible to spontaneous tumours. *Nature* **356**: 215–221.

Donev A, Cisse I, Sachs D *et al.* (2004) Improving the density of jammed disordered packings using ellipsoids. *Science* **303**: 990–993.

Dundr M, Misteli T (2001) Functional architecture in the cell nucleus. *Biochem J* **356**: 297–310.

Gilbert N, Boyle S, Fiegler H, Woodfine K, Carter NP, Bickmore WA (2004) Chromatin architecture of the human genome: gene-rich domains are enriched in open chromatin fibers. *Cell* **118**: 555–566.

Gilbert N, Gilchrist S, Bickmore WA (2005) Chromatin organization in the mammalian nucleus. *Int Rev Cytol* **242**: 283–336.

Hlatky L, Sachs RK, Vazquez M, Cornforth MN (2002) Radiation-induced chromosome aberrations: insights gained from biophysical modeling. *Bioessays* **24**: 714–723.

Hochberg Y (1988) A sharper Bonferroni procedure for multiple tests of significance. *Biometrika* **75**: 800–802.

Hope ACA (1968) A simplified Monte Carlo significance test procedure. *Journal of the Royal Statistical Society B* **30**: 582–598.

Khalil A, Grant JL, Caddle LB, Aztema E, Mills KD, Arneodo A (2007) Chromosome territories have a highly nonspherical morphology and nonrandom positioning. *Chromosome Res.* **15**: 899–916.

Kreth G, Finsterle J, von Hase J, Cremer M, Cremer C (2004) Radial arrangement of chromosome territories in human cell

nuclei: a computer model approach based on gene density indicates a probabilistic global positioning code. *Biophys J* **86**: 2803–2812.

Meaburn KJ, Misteli T (2007) Cell biology: chromosome territories. *Nature* **445**: 379–781.

Meaburn K, Misteli JT, Soutoglou E (2007) Spatial genome organization in the formation of chromosomal translocations. *Semin Cancer Biol* **17**: 80–90.

Mills KD, Ferguson DO, Essers J, Eckersdorff M, Kanaar R, Alt FW (2004) Rad54 and DNA Ligase IV cooperate to maintain mammalian chromatid stability. *Genes Dev* **18**: 1283–92.

Mora L, Sanchez I, Garcia M, Ponsa M (2006) Chromosome territory positioning of conserved homologous chromosomes in different primate species. *Chromosoma* **115**: 367–375.

Murmann AE, Gao J, Encinosa M *et al*. (2005) Local gene density predicts the spatial position of genetic loci in the interphase nucleus. *Exp Cell Res* **311**: 14–26.

Osborne CS, Chakalova L, Mitchell JA *et al*. (2007) Myc dynamically and preferentially relocates to a transcription factory occupied by Igh. *PLoS Biol* **5**: e192.

Parada L, Misteli T (2002) Chromosome positioning in the interphase nucleus. *Trends Cell Biol* **12**: 425–432.

Parada LA, McQueen PG, Misteli T (2004a) Tissue-specific spatial organization of genomes. *Genome Biol* **5**: R44.

Parada LA, Sotiriou S, Misteli T (2004b) Spatial genome organization. *Exp Cell Res* **296**: 64–70.

Shopland LS, Lynch CR, Peterson KA *et al*. (2006) Folding and organization of a contiguous chromosome region according to the gene distribution pattern in primary genomic sequence. *J Cell Biol* **174**: 27–38.

Stadler S, Schnapp V, Mayer R *et al*. (2004) The architecture of chicken chromosome territories changes during differentiation. *BMC Cell Biol* **5**: 44.

Tanabe H, Muller S, Neusser M *et al*. (2002) Evolutionary conservation of chromosome territory arrangements in cell nuclei from higher primates. *Proc Natl Acad Sci USA* **99**: 4424–4429.

Thomson I, Gilchrist S, Bickmore WA, Chubb JR (2004) The radial positioning of chromatin is not inherited through mitosis but is established *de novo* in early G1. *Curr Biol* **14**: 166–172.